Tutorial Vol. 37, No. 4 / April 2020 / Journal of the Optical Society of America A 591

Journal of the Optical Society of America A

OPTICS, IMAGE SCIENCE, AND VISION

Synthesis and characterization of non-uniformly totally polarized light beams: tutorial

GEMMA PIQUERO,[1] ROSARIO MARTÍNEZ-HERRERO,[1] J. C. G. DE SANDE,[2,*] AND MASSIMO SANTARSIERO[3]

[1]Departamento de Óptica, Universidad Complutense de Madrid, Ciudad Universitaria, 28040 Madrid, Spain
[2]ETSIS de Telecomunicación, Universidad Politécnica de Madrid, Nikola Tesla s/n Campus Sur, 28031 Madrid, Spain
[3]Dipartimento di Ingegneria, Università Roma Tre, Via V. Volterra 62, 00146 Rome, Italy
*Corresponding author: juancarlos.gonzalez@upm.es

Received 9 October 2019; revised 5 February 2020; accepted 10 February 2020; posted 10 February 2020 (Doc. ID 379439); published 17 March 2020

Polarization of a light beam is traditionally studied under the hypothesis that the state of polarization is uniform across the transverse section of the beam. In such a case, if the paraxial approximation is also assumed, the propagation of the beam reduces to a scalar problem. Over the last few decades, light beams with spatially variant states of polarization have attracted great attention, due mainly to their potential use in applications such as optical trapping, laser machining, nanoscale imaging, polarimetry, etc. In this tutorial, an introductory treatment of non-uniformly totally polarized beams is given. Besides a brief review of some useful parameters for characterizing the polarization distribution of such beams across transverse planes, from both local and global points of view, several methods for generating them are described. It is expected that this tutorial will serve newcomers as a starting point for further studies on the subject.

https://doi.org/10.1364/JOSAA.379439

1. INTRODUCTION

Polarization of light is an exciting subject, and numerous books and research articles have been devoted to understanding and modeling this characteristic of light, even in very recent times [1–13].

Elementary approaches to polarization generally make reference to the direction of the electric field vector of a plane wave, for which the polarization state is assumed to be uniform all over in the space. Uniform polarization is also generally assumed in the study of light beams. In more general situations, however, the polarization of a beam may vary from one point to another of its cross section, thus giving rise to the so-called *non-uniformly polarized* (NUP) beams. Early works on this subject dealt with the generation of NUP beams by interferometric methods [14,15] or at the output of semiconductor lasers [16]. Then the need arose, on one hand, to devise methods for synthesizing fields presenting peculiar polarization patterns across their transverse section and, on the other hand, to model and characterize the polarization of such beams.

We refer to those beams that present complete polarization at any point (although not uniform) as *non-uniformly totally polarized* (NUTP) beams. Many different kinds of NUTP beams have been introduced over the last few decades [17–45]. In particular, radially and azimuthally polarized beams, spirally polarized beams (SPBs), and full Poincaré beams (FPBs) have been extensively studied [5,17,25,29,39,40,44–51]. The introduction of NUTP beams has been followed by their use in numerous application fields, such as optical tweezers, particle optical manipulation, material processing, microscopy, focus shaping, surface plasmon sensing, polarimetry, etc. [10,12,13,25,44,52–70].

In this tutorial, we report on some aspects of the research on NUTP beams related to their synthesis and their theoretical and experimental characterization. Due to the vastness and the fast development of the techniques in this field, unavoidably many important works and applications will be not recalled in this tutorial. What we are going to present is a selection of simple tools for the synthesis and characterization of NUTP beams, each of them accompanied by the description of its experimental implementation, that could be realized with conventional optical systems and do not require sophisticated or expensive equipment. We think the presented techniques can be of help to new researchers and can attract their attention and interest to this subject, and may also represent the starting point for envisaging more complex synthesis methods for these or more general NUP beams. Some aspects will not be covered, such as the ones related to partially coherent and/or nonparaxial fields, in which cases interesting properties and effects have also been found (see, e.g., [71–73]). In fact, we will consider only fields perfectly coherent from the spatial point of view, and paraxial

conditions will always be taken for granted, so that the term *beam* is justified when dealing with their propagation.

The paper is structured as follows: after this introductory section, the parameters used to describe the polarization of a light field are briefly recalled (Section 2). Some local and global parameters aimed at characterizing NUP beams are presented in Section 3, and different methods to synthesize some types of NUTP beams are described in Section 4. Finally, in Section 5 a brief summary is given.

2. CHARACTERIZING POLARIZATION OF LIGHT

Here, we give a short review of the parameters that are commonly used to describe the polarization of light, and that will be used throughout the paper.

If we limit ourselves to light fields propagating in paraxial conditions (along the z axis of a suitable reference frame), the longitudinal component of their electric field can be neglected, and the characterization of their polarization at any point requires only the knowledge of the complex amplitudes of the two transverse components, namely, E_x and E_y [1–4,74].

Under such conditions, the expression of the electric field of a beam at a typical point in space is

$$\mathbf{E}(t) = \left[E_x(t)\mathbf{u}_x + E_y(t)\mathbf{u}_y\right] e^{i\omega t}, \tag{1}$$

where $\mathbf{u}_j$ (with $j = x, y$) are unitary vectors along the j direction, and ω is the angular frequency. Here, for simplicity we have omitted the explicit dependence on the point location, but it should be clear that, in general, E_x and E_y depend on it. Furthermore, if the radiation is not strictly monochromatic, E_x and E_y depend also on time. Nonetheless, for quasi-monochromatic light, they vary over times that are much longer than the oscillation period of the radiation and can be considered practically constants within a period.

Therefore, at any considered point, the electric field is the superposition of two orthogonal harmonic oscillators, and its tip describes, in a complete period, an ellipse. The latter is referred to as the *polarization ellipse* of the light. Depending on the amplitudes and phases of the field components, such an ellipse can degenerate into a circle (*circular* polarization) or a line (*linear* polarization). The shape of the ellipse and the sense in which the electric field vector moves are determined completely by the ratio between the complex quantities E_x and E_y, i.e., by the ratio of their absolute values and by their relative phase.

Note that in general, the transverse polarization pattern of a beam evolves during propagation (see, e.g., [71,75–81]), and the way it changes depends on the spatial distributions of both the complex quantities E_x and E_y, and not only on the ratio of their absolute values and their relative phase. This means that in general, the polarization profile of a beam across a transverse plane is not sufficient for determining its polarization across other planes.

The amplitudes of the transverse component of the electric field are often arranged into a single 2×1 vector, i.e.,

$$\mathbf{E} = \begin{pmatrix} E_x \\ E_y \end{pmatrix}, \tag{2}$$

which is usually referred to as the *Jones vector* of the field [1,2,4]. A deterministic linear optical system can be represented by a 2×2 complex matrix, $\hat{T}$, known as the *Jones matrix*, which transforms the electric field components of a beam in a linear way when it passes through the system, i.e.,

$$\mathbf{E}^{\text{out}} = \hat{T}\,\mathbf{E}^{\text{in}}, \tag{3}$$

thus modifying its polarization state. Note that the Jones matrix of a homogeneous system does not depend on the position, so that it transforms the input state of polarization in the same way across its whole section.

Except for a scale factor, the ellipse of polarization can be described by two angles ψ and χ, representing the azimuth of the major axis relative to the x axis and the ellipticity angle of the ellipse, respectively. Azimuth and ellipticity angles are related to the electric field components by the relations [2,4,74]

$$\psi = \frac{1}{2}\arctan\left(\frac{2\text{Re}\{E_x^* E_y\}}{|E_x|^2 - |E_y|^2}\right) \tag{4}$$

and

$$\chi = \frac{1}{2}\arcsin\left(\frac{2\text{Im}\{E_x^* E_y\}}{|E_x|^2 + |E_y|^2}\right), \tag{5}$$

where the asterisk denotes complex conjugation and Re{·} (Im{·}) the real (imaginary) part of a complex number. The azimuth, ψ, can assume values within the interval $[0, \pi)$, while the ellipticity, χ, is limited to the range $(-\pi/4, \pi/4]$ [2,4,74]. The sign of χ denotes the sense in which the ellipse of polarization is traced out, being right-handed (left-handed) if $\chi > 0$ ($\chi < 0$).

Now, by taking a point with spherical coordinates $(1, 2\psi, \pi/2 - 2\chi)$ in a 3D space, any given pair of azimuth and ellipticity can be graphically represented as a point on the surface of a sphere with unit radius. Such a sphere is known as the *Poincaré sphere* (see Fig. 1). The rectangular coordinates of a point in this space are denoted by s_1, s_2, s_3 and are referred to as the *normalized Stokes parameters* of the field. The equator of the sphere ($s_3 = 0$) contains all the linear polarization states, while the north (south) pole represents right-handed (left-handed) circularly polarized light ($s_3 = 1$ and $s_3 = -1$, respectively). A generic point on the north (south) hemisphere represents a right-handed (left-handed) elliptical state of polarization.

For a perfectly monochromatic field, the amplitudes E_x and E_y do not change with time, so the parameters specifying the polarization are constant, too. On the contrary, in practical cases, they are constant only within time intervals much shorter than the coherence time of the radiation, which, in turn, is related to the width of its power spectrum [82]. For longer time intervals, they are expected to change. Therefore, the ratio between the absolute values of the amplitudes of the field components, as well as their relative phase, may fluctuate, and the representative point on the Poincaré sphere is expected to move. Typically, response times of the instruments used to detect light radiation are much longer than the coherence time of the radiation itself, so only average values of the above quantities are accessible in practice. In particular, only the mean position

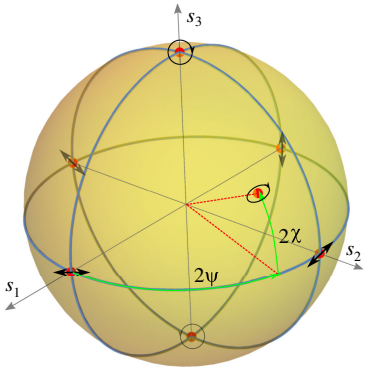

Fig. 1. Poincaré sphere. Any point on its surface corresponds to a different polarization state.

of the point moving on the Poincaré sphere is detectable, and the coordinates of such position correspond to the normalized Stokes parameters of the field.

The right tool for taking light fluctuations into account is the *polarization matrix*, $\hat{P}$, which is evaluated from the electric field components as [82,83]

$$\hat{P} = \begin{pmatrix} P_{xx} & P_{xy} \\ P_{yx} & P_{yy} \end{pmatrix}, \tag{6}$$

where

$$P_{ij} = \langle E_i^*(t) E_j(t) \rangle, \tag{7}$$

with $i, j = x, y$. Here, the brackets represent a time average performed over a sufficiently long time, compared to the typical times in which the random variables that define the field change. Stochastic processes are supposed to be stationary, so that the elements of $\hat{P}$ are independent of time. Using the Schwarz inequality, it can be shown that $\hat{P}$ is a semi-positive definite matrix [82,83].

From the elements of the matrix $\hat{P}$, the *Stokes parameters* of the field can be defined as [1–5,7,8,74]

$$\begin{aligned} S_0 &= P_{xx} + P_{yy}, \\ S_1 &= P_{xx} - P_{yy}, \\ S_2 &= 2\mathrm{Re}\{P_{xy}\}, \\ S_3 &= 2\mathrm{Im}\{P_{xy}\}, \end{aligned} \tag{8}$$

which are usually arranged into a 4×1 vector called the *Stokes vector*.

It is important to stress that the Stokes parameters are real quantities and can be obtained by measuring the irradiance of the field after suitable oriented linear polarizers and retardation plates. In fact, it turns out that

$$\begin{aligned} S_0 &= I_0 + I_{\pi/2} \\ S_1 &= I_0 - I_{\pi/2}, \\ S_2 &= I_{\pi/4} - I_{-\pi/4}, \\ S_3 &= I'_{\pi/4} - I'_{-\pi/4}, \end{aligned} \tag{9}$$

where I_θ and I'_θ are the irradiances measured, respectively, after a linear polarizer oriented at the angle θ and after a quarter-wave phase plate followed by the linear polarizer [1,2,4].

The first Stokes parameter, S_0, provides the irradiance of the beam, and the normalized Stokes parameters are obtained dividing the last three Stokes parameters by S_0, i.e.,

$$s_n = \frac{S_n}{S_0}, \quad (n = 1, 2, 3). \tag{10}$$

The most significant effect of the fluctuations of the field components is that, as could be expected, the point whose coordinates are given by the relations in Eq. (10), in general, no longer belongs to the surface of the Poincaré sphere, but may be also located inside the sphere. In fact, it turns out that $s_1^2 + s_2^2 + s_3^2 \leq 1$. The radial coordinate of such point is taken as a measure of the *degree of polarization* of the field, i.e.,

$$\mathcal{P} = \sqrt{s_1^2 + s_2^2 + s_3^2}. \tag{11}$$

A field is said *totally* (or *perfectly*) *polarized* when $\mathcal{P} = 1$. In such a case, perfect correlation exists between the two transverse components of the electric field, so that the polarization state of the field does not change with time. In the opposite limit ($\mathcal{P} = 0$), the field is *completely unpolarized*. This happens when the two transverse field components are completely uncorrelated and carry the same power. In all other cases, the field is said to be *partially polarized*.

It should be noted that any partially polarized field can be expressed as the sum of two fields: a totally polarized and an unpolarized field. This is a consequence of the fact that the polarization matrix of any field can be decomposed into two terms, one of them proportional to the 2×2 identity matrix (representing the unpolarized component), and the other one describing the completely polarized component [84,85]. Making use of this decomposition, the degree of polarization can be interpreted as the ratio between the irradiance of the totally polarized component and the total irradiance.

3. CHARACTERIZING NUTP BEAMS

Standard approaches to polarization often assume the polarization of a light beam to be uniform across the beam transverse section, and this single polarization is also preserved during paraxial propagation. In the more general case of a NUTP beam, representing its polarization is more demanding because the polarization matrix depends on the position across the transverse plane. Moreover, as stated above, the transverse polarization distribution of a beam generally changes during propagation, so that a complete (i.e., all over the space) characterization of the polarization of a NUTP beam would require the determination of the polarization pattern across a set, virtually infinite, of transverse planes.

The characterization of the polarization distribution in NUTP beams will be performed starting from the quantities recalled in the previous section. Some global parameters, which can be obtained from the values (both calculated or measured) of the Stokes parameters, will also be defined.

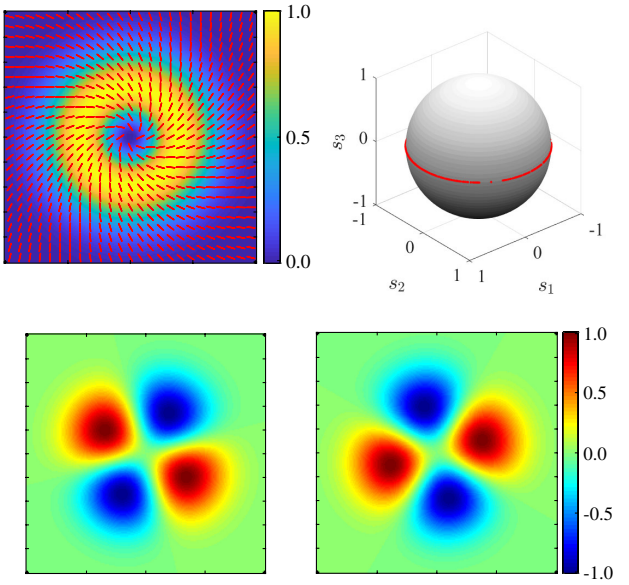

Fig. 2. SPB beam with $\gamma = \pi/6$. Upper row: polarization pattern where the red segments indicate the azimuth of the linear polarization (left) and representation of the corresponding state of polarization by means of red dots on the Poincaré sphere (right). Lower row: Stokes parameters S_1 (left) and S_2 (right).

A. Local Characterization

The polarization of a NUP beam can be represented, at each plane $z =$ constant, by 2D plots of the four Stokes parameters or, alternatively, by plots of the degree of polarization and of three parameters describing the polarization state of the totally polarized component of the field. Since NUTP beams have $\mathcal{P} = 1$ everywhere, their polarization is described completely by the latter three parameters and can be represented graphically by ellipses at selected points of the beam cross section, as done in Figs. 2–4.

As a simple example of a NUTP beam we consider a SPB [17], whose Jones vector is

$$\mathbf{E}_{\mathrm{SP}}(\mathbf{r}) = f(r) \begin{pmatrix} \cos(\theta + \gamma) \\ \sin(\theta + \gamma) \end{pmatrix}, \tag{12}$$

where (r, θ) are the polar coordinates of a typical point across a transverse plane, and γ is a constant angle. The function $f(r)$ gives the spatial distribution of the irradiance and must vanish at the point $r = 0$ because the polarization is not defined there.

A beam of the form in Eq. (12) presents cylindrical symmetry around the z axis, and its polarization state is linear at any point. The electric field lines are logarithmic spirals whose growth parameter depends on the value of γ [17]. On varying γ, different patterns of the polarization across the beam section are obtained, ranging from radial (when $\gamma = 0$) to azimuthal (when $\gamma = \pi/2$) polarization (see Fig. 2) [17,26,75,77,79,86]. It is important to note that the polarization pattern of beams of this kind remains unchanged during free-space propagation.

Figure 2 shows the polarization pattern, the Stokes parameters, and the representation of the corresponding states of polarization on the surface of the Poincaré sphere for the case of a SPB with $\gamma = \pi/6$. The field amplitude has been chosen as $f(r) \propto r \exp(-r^2/w_0^2)$, w_0 being related to the beam waist size. The polarization pattern has been superimposed to the irradiance profile of the beam (S_0 normalized to its maximum), while the Stokes parameters S_1 and S_2 have been normalized to the maximum beam irradiance. Note that $S_3 = 0$ for this kind of beam. On the Poincaré sphere, the red dots correspond to the states of polarization plotted in the polarization pattern. These red points lay on the equator of the Poincaré sphere, and some space among them can be noted due to the sampling of the polarization pattern across the beam section. With a higher sampling rate, red points cover in a more compact way the whole equator.

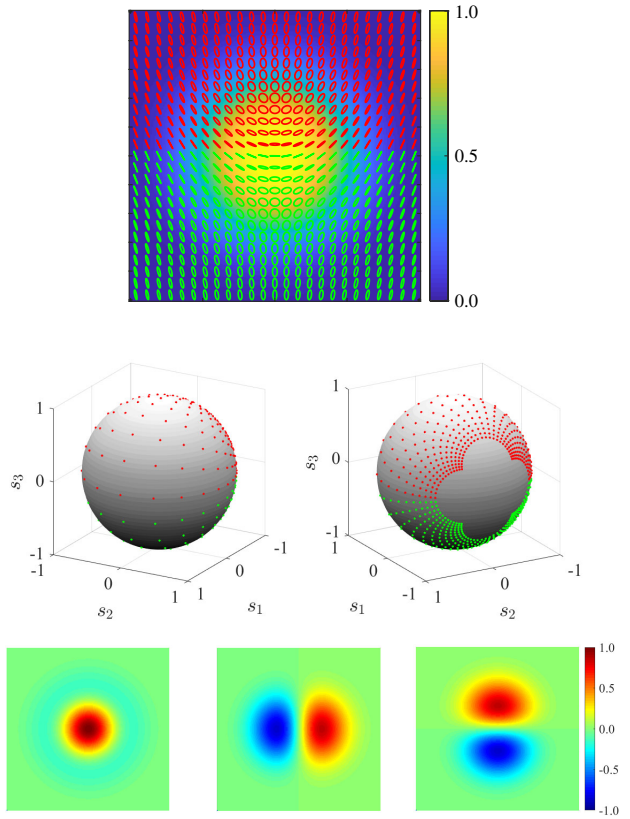

Fig. 3. Polarization pattern (top) for the FPB given by Eq. (13) with $\Phi = \pi/4$; two views of such pattern on the Poincaré sphere (middle); and Stokes parameters S_1, S_2, and S_3, from left to right, normalized to the maximum irradiance of the beam (bottom). Red (green) ellipses and dots denote right-handed (left-handed) polarization.

Another family of NUTP beams that has attracted great interest is that of the so-called FPBs [46], which present all possible totally polarized states of polarization in their cross sections. In other words, the polarization state pattern of a FPB maps the entire Poincaré sphere surface at least once. For example, the Jones vector at the plane $z = 0$ can be chosen as the following superposition of Laguerre–Gaussian modes [46]:

$$\mathbf{E}_{\mathrm{FP}_0}(\mathbf{r}) = E_0 \exp\left(-\frac{r^2}{w_0^2}\right) \begin{pmatrix} \cos\Phi \\ \frac{\sqrt{2}r}{w_0} e^{i\theta} \sin\Phi \end{pmatrix}, \tag{13}$$

where E_0 is an amplitude factor, w_0 is the common waist size of the modes, and Φ is a parameter that determines the weight

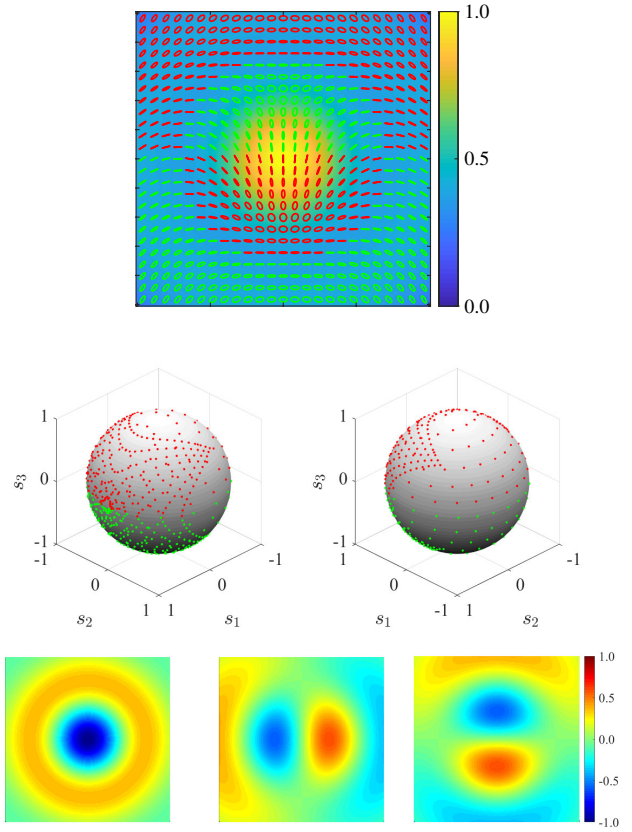

Fig. 4. Polarization pattern (top) for the FPB given by Eq. (14) with $\Phi = \pi/4$; two views of such pattern on the Poincaré sphere (middle); and Stokes parameters S_1, S_2, and S_3, from left to right, normalized to the maximum irradiance of the beam (bottom). Red (green) ellipses and dots denote right-handed (left-handed) polarization.

of each mode in the superposition. This kind of FPB has been experimentally generated by means of a symmetrically stressed optical window (see [33,46] and references therein). Figure 3 shows the resulting polarization pattern for $\Phi = \pi/4$, together with the Stokes parameters and the states of polarization represented as points on the Poincaré sphere.

It must be noted that in such a FPB, the polarization states across the cross section correspond to a stereographic projection of the Poincaré sphere from the point $(-1, 0, 0)$ [46]. We calculated and represented only a finite-sized (squared) region of the cross section, so that a portion of this projection is lost. This can be noticed when the corresponding polarization states are represented on the Poincaré sphere: no polarization states are found in the region around $s_1 = -1$. We considered a grid of 25×25 points, so that only 625 points are shown on the Poincaré sphere, but a higher sampling rate of the beam cross section would result in a denser covering of the surface of the Poincaré sphere, without extending the covered region.

A FPB that shows all possible polarization states in a finite region of its transverse section can be obtained by the superposition of two orthogonally polarized Laguerre–Gauss modes with, at least, a radial index greater than zero, such as the following one [48]:

$$\mathbf{E}_{\mathrm{FP}_1}(\mathbf{r}) = E_0 \exp\left(-\frac{r^2}{w_0^2}\right)\begin{pmatrix} \frac{r}{w_0}\mathrm{e}^{\mathrm{i}\theta}\cos\Phi \\ \left(1-\frac{2r^2}{w_0^2}\right)\sin\Phi \end{pmatrix}. \tag{14}$$

Figure 4 shows the polarization pattern of the FPB generated by Eq. (14) and two views of their representation on the Poincaré sphere. The profile of the Stokes parameters S_1, S_2, and S_3 are also shown. In this case, all possible states of polarization are found in a finite circular region of radius $r_0 = w_0/\sqrt{2}$ [48]. The two examples of FPB described by Eqs. (13) and (14) belong to a wide class of FPBs that can be generated by superposition of two orthogonally polarized Laguerre–Gauss modes of different orders [46,48].

From the experimental point of view, local characterization implies measurements in a finite-sized region that could be small, but not pointlike. A pinhole can be placed in front of the detector in such a way that the detection area could be made small enough to consider the state of polarization almost uniform within the detector area. When the detection system is a digital camera, the size of the pixels should be small enough, compared to the area where the polarization state remains almost the same. In any case, for a local characterization of a NUTP, a lot of points have to be analyzed, and very large arrays of states of polarization are involved.

B. Global Characterization

Up to now, the characterization of a NUTP light beam has been approached from the local point of view, using different representations of the polarization. In many applications, however, the knowledge of the detailed structure of a polarization pattern it is not strictly necessary, and the only useful information that can be contained is some global parameters. Examples of global parameters for characterizing NUTP beams are given below.

1. Weighted Degree of Polarization

From the local degree of polarization, $\mathcal{P}(\mathbf{r})$, the *weighted degree of polarization* can be defined as [74,87,88]

$$\widetilde{\mathcal{P}} = \frac{1}{I_T}\int \mathcal{P}(\mathbf{r}) S_0(\mathbf{r})\mathrm{d}\mathbf{r}, \tag{15}$$

where the integration is extended to the whole transverse plane, and

$$I_T = \int S_0(\mathbf{r})\mathrm{d}\mathbf{r} \tag{16}$$

is the total power of the beam. We recall that the Stokes parameters $S_0(\mathbf{r})$ give the local irradiance of the beam, so the weighted degree of polarization gives the average over the region of the beam cross section where the irradiance is significant.

To evaluate the uniformity of the local degree of polarization across the transverse beam profile, the variance σ_p^2 of the previous parameter can be used, which is defined as [74,87]

$$\sigma_p^2 = \frac{1}{I_T}\int [\mathcal{P}(\mathbf{r}) - \widetilde{\mathcal{P}}]^2 S_0(\mathbf{r})\mathrm{d}\mathbf{r}. \tag{17}$$

It is easy to show that $0 \le \sigma_p^2 \le 1/2$ [74,87].

Of course, for a perfect NUTP beam, it must be $\widetilde{\mathcal{P}} = 1$ and $\sigma_p = 0$. Therefore, measuring these two parameters allows one to determine how close a NUP beam is to a NUTP beam.

2. Circular Polarization Content

The information provided by the weighted degree of polarization can be complemented by another global parameter that measures the content of circularly polarized light in a NUTP beam [74,89]. This parameter is defined as

$$\rho_c = \frac{1}{I_T}\int S_3(\mathbf{r})\mathrm{d}\mathbf{r} \tag{18}$$

and can take values from −1 (pure left-handed circularly polarized beam) to 1 (pure right-handed circularly polarized beam). The uniformity of the circularly polarized content of a beam can be evaluated through the variance of the values of ρ_c, which is defined as

$$\sigma_c^2 = \frac{1}{I_T}\int \left[\frac{S_3(\mathbf{r})}{S_0(\mathbf{r})} - \rho_c\right]^2 S_0(\mathbf{r})\mathrm{d}\mathbf{r}. \tag{19}$$

It is clear that for NUTP beams presenting only linear polarization states, it will be $\rho_c = \sigma_c = 0$. This is the case of the SPB in Eq. (12), which, regardless of the parameter γ, is linearly polarized everywhere. Regarding the two FPBs described by Eqs. (13) and (14), the circular polarization content is zero for both of them. This means that right and left handedness are equally represented across the beam cross section. The variances of the circular polarization content turn out to be 0.40 for the first case and 0.35 for the second one.

3. Radial/Azimuthal Polarization Content

The parameter ρ_c does not allow to distinguish between fields showing linearly polarized states with different azimuths, such as SPBs with different parameters γ. On the contrary, in some cases, it would be interesting to know the content of radial or azimuthal polarization of the beam across a certain plane. To this aim, the following two global parameters can be defined as [74,90,91]

$$\begin{aligned}\rho_R = &\frac{1}{2} + \frac{1}{2I_T}\int_0^\infty\int_0^{2\pi}\cos(2\theta)S_1(r,\theta)r\,\mathrm{d}r\,\mathrm{d}\theta \\ &+\frac{1}{2I_T}\int_0^\infty\int_0^{2\pi}\sin(2\theta)S_2(r,\theta)r\,\mathrm{d}r\,\mathrm{d}\theta, \\ \rho_A = &\frac{1}{2} - \frac{1}{2I_T}\int_0^\infty\int_0^{2\pi}\cos(2\theta)S_1(r,\theta)r\,\mathrm{d}r\,\mathrm{d}\theta \\ &-\frac{1}{2I_T}\int_0^\infty\int_0^{2\pi}\sin(2\theta)S_2(r,\theta)r\,\mathrm{d}r\,\mathrm{d}\theta.\end{aligned} \tag{20}$$

The parameter ρ_R (ρ_A) provides the content of radially (azimuthally) polarized light of the beam and can take values from zero to one, this last case corresponding to a pure radially (azimuthally) polarized beam. Note that for NUTP beams, the relation $\rho_R + \rho_A = 1$ holds.

For a SPB [see Eq. (12)], the radially and azimuthally polarized light contents are independent of the field amplitude $f(r)$ and turn out to be [26,27]

$$\rho_R = \frac{1}{2} - \frac{1}{2}\cos(\gamma) \tag{21}$$

and

$$\rho_A = \frac{1}{2} + \frac{1}{2}\cos(\gamma), \tag{22}$$

respectively.

Finally, for both types of FPBs in Eqs. (13) and (14), $\rho_A = \rho_R = 1/2$.

4. SYNTHESIZING NUTP BEAMS

Several methods have been proposed and carried out to experimentally synthesize different types of NUP beams. They use Mach–Zehnder interferometers (MZIs), fiber lasers running in either CW or pulsed mode, digital lasers, spatial light modulators (SLMs), metasurfaces, stressed optical windows, q-plates, spiral phase plates, photoaligned liquid crystals, digital micromirrors, and more (see, e.g., [6,23,25,28,33,46,52,57,61,66,69,92–95]). In this tutorial, we will describe some techniques to generate NUTP beams that could be implemented with conventional optical systems and do not require sophisticated optical equipment, such as SLMs, or complex configurations, such as modifications of a laser cavity, and so on.

In particular, we will focus our attention on three methods, based on different approaches: the use of spatially varying polarizers, of interferometric systems, and of anisotropic crystals. We shall give a detailed description of some experimental setups aimed at producing NUTP beams, and hints for their characterization.

A. Spatially Varying Anisotropic Elements

Conventional anisotropic optical elements, such as wave plates and polarizers, are homogeneous, in the sense that their Jones matrix is uniform across their surface. When illuminated by a uniformly polarized beam, they always produce a uniformly polarized beam as their output. However, it is possible to envisage spatially varying anisotropic elements whose characteristics depend on the position across their surface. It is clear that in such a case, a uniformly polarized beam impinging onto this optical element is converted into a NUTP beam.

Polarization gratings [96–103] are examples of these kinds of elements. They behave like polarizers, but their transmission axis is oriented along a direction that varies in a periodic way along a transverse direction. For example, if the transmission angle varies linearly with the coordinate of the x axis, the following Jones matrix is obtained:

$$\hat{T}_{\mathrm{PG}}(\mathbf{r}) = \begin{pmatrix} \cos^2\beta x & \cos\beta x\sin\beta x \\ \cos\beta x\sin\beta x & \sin^2\beta x \end{pmatrix}, \tag{23}$$

where $\beta = 2\pi/L$, L being the grating period.

If the incident beam has uniform amplitude E_0 and is circularly polarized (e.g., right), the amplitude of the output beam is uniform, too, but the polarization state is the one imposed by the grating, i.e.,

$$\mathbf{E}_{\mathrm{PG}}(\mathbf{r}) = \frac{E_0}{\sqrt{2}}e^{\mathrm{i}\beta x}\begin{pmatrix}\cos\beta x \\ \sin\beta x\end{pmatrix}. \tag{24}$$

A simple, approximated version of a polarization grating can be realized by juxtaposing thin strips cut from a polarizing film. More sophisticated techniques require the use of space-variant subwavelength dielectric gratings [101,104]. In the latter case, of course, a wider class of spatially varying optical elements can be obtained [105,106], at the cost of greater construction difficulties.

Another simple, commercially available element behaves as a linear polarizer having the transmission axis oriented along the azimuthal direction. Its Jones matrix is of the form

$$\hat{T}_{\mathrm{AP}}(\mathbf{r}) = \begin{pmatrix} \sin^2\theta & -\cos\theta\sin\theta \\ -\cos\theta\sin\theta & \cos^2\theta \end{pmatrix} \tag{25}$$

and is used as a *polarization axis finder* (see, e.g., Edmund Optics or TSI Incorporated). When illuminated by a right-handed circularly polarized beam with circularly symmetric amplitude $f(r)$, it produces the field

$$\mathbf{E}_{\mathrm{AP}}(\mathbf{r}) = \frac{\mathrm{i}}{\sqrt{2}} f(r)\, e^{\mathrm{i}\theta} \begin{pmatrix} -\sin\theta \\ \cos\theta \end{pmatrix}. \tag{26}$$

Note that although the polarization direction of the output beam is along the azimuthal direction at any point of the transverse section, its form is not the same as in Eq. (12) because of the presence of the term $\exp(i\theta)$, so the transverse polarization distribution changes during propagation [17].

To obtain a beam with cylindrical symmetry (with azimuthal, radial, or, more generally, spiral-like polarization) different optical elements can be used [14–16,23,25,26,28,101,107]. One of them is commercially available as a *polarization converter* [107]. It consists of a blend of nematic liquid crystal cells placed between two alignment layers: one of them linearly rubbed along a given direction and the other rubbed in a concentric-circle pattern. The nematic liquid crystals' alignment inside the cell changes from the linear to the azimuthal pattern, and so an azimuthally polarized output beam is obtained when a linearly polarized light impinges on the linearly rubbed alignment layer of the cell [107].

A polarization converter (PC) with its input and output faces perpendicular to the z axis (the assumed direction of propagation of the input beam) and the linearly rubbed layer oriented along the y direction, when illuminated by light linearly polarized along y with circularly symmetric amplitude $f(r)$, produces at the exit plane the field [107]

$$\mathbf{E}_{\mathrm{PC}}(\mathbf{r}) = f(r) \begin{pmatrix} -\sin\theta \\ \cos\theta \end{pmatrix}, \tag{27}$$

which is of the form in Eq. (12) with $\gamma = \pi/2$.

The field obtained in such a way can be used to produce a spirally polarized beam with arbitrary parameter γ. The details of some of the synthesis procedures and a technique for their characterization are described in the next subsection.

1. Synthesis of SPBs

The experimental setup used to produce a SPB is shown in Fig. 5. The light emerging from a He–Ne laser, linearly polarized along the vertical direction, is expanded and enters the PC. An azimuthally polarized beam is obtained at the exit of the PC and is spatially filtered by means of a system consisting of a microscope objective, a spatial filter (SF), and a converging lens. To convert it into a SPB, a polarization rotator (R) is used. The latter rotates the electric field of the incident field of the angle γ' and consists of two half-wave phase plates forming an angle $\gamma'/2$ between them [26,77], as shown in the inset of Fig. 5. By selecting $\gamma' = \pi/2 + \gamma$, the resulting field is like the one described in Eq. (12). In the latter figure, although most of the polarization states appear to be linear, according to their color, all of them are denoted as either left- or right-handed. This is due to the fact that the figure reports experimental values, and the measured values of s_3 can be arbitrarily small, but hardly ever vanishing.

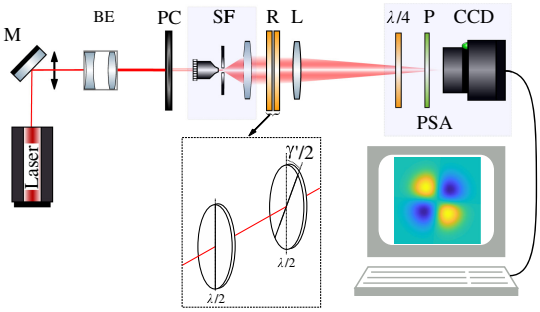

Fig. 5. Experimental scheme for synthesizing SPBs. BE, beam expander; PC, polarization converter; SF, spatial filter; R, rotator; L, lens; PSA, polarization state analyzer composed of a quarter-wave phase plate ($\lambda/4$), a dichroic polarizer P, and a CCD camera.

Finally, a convergent lens (L) is placed to form the image of the field emerging from the rotator on a CCD camera, used to perform the analysis of the polarization distribution across the beam section.

The experimental polarization patterns have been obtained by means of a simple polarization state analyzer (PSA), consisting of a quarter-wave plate, a linear polarizer, and a CCD camera. The local Stokes parameters of the beam were measured in the following way: four images of the beam section were captured after a linear polarizer with different orientations of its transmission axis (0, $\pm\pi/4$, and $\pi/2$ with respect to the x axis), and two additional images werer recorded when a quarter-wave phase plate, having its fast axis along the x direction, was inserted before the polarizer (the latter with its axis at $\pm\pi/4$). The irradiance values contained in the recorded images were inserted into Eq. (9), from which the local Stokes vector and the corresponding polarization ellipse at each point were evaluated. A representation of the measured polarization patterns is shown in Fig. 6.

By changing the value of γ from zero to π radians, various spiral-type polarization patterns can be obtained. In particular, $\gamma = 0$ and $\gamma = \pi$ lead to an azimuthal polarization distribution, while $\gamma = \pi/2$ gives rise to a radially polarized beam.

The global parameters corresponding to the experimentally generated SPB shown in Fig. 6 turn out to be $\tilde{\mathcal{P}} = 0.97$, $\sigma_p^2 = 0.01$, $\rho_c = 0.08$, $\sigma_c^2 = 0.01$, $\rho_R = 0.11$, and $\rho_A = 0.89$, which are quite close to the theoretical ones for a SPB with $\gamma = 20°$.

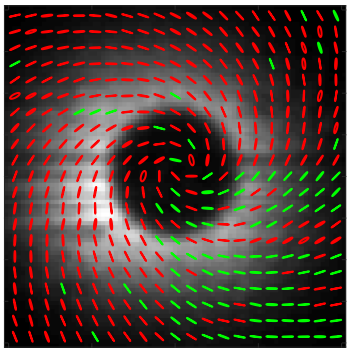

Fig. 6. Experimental spirally polarized pattern with $\gamma = 20°$. Red (green) ellipses denote right-handed (left-handed) polarization states.

B. Interferometers

The mathematical form of a Jones vector itself suggests a way to synthesize any NUTP beam: it will be sufficient to superimpose two suitably chosen mutually coherent, uniformly polarized beams having orthogonal polarization states. Since the two component beams must be mutually coherent, they can be produced through interferometric techniques. In general, of course, to obtain a NUTP beam, the two replicas produced by the interferometer must differ in the irradiance and/or in the phase profile. This was indeed one of the first techniques used to synthesize NUTP beams. In Ref. [15], for instance, two Hermite Gaussian modes, of orders (0,1) and (1,0), respectively, with orthogonal linear polarizations, were superimposed by means of a MZI to produce a radially polarized beam with uniform azimuthal irradiance.

Several different interferometric configurations have been proposed in subsequent years to produce NUTP fields. Among them, we quote the techniques using Fresnel biprisms [108], Young double slits [109], diffractive optical elements [110], Sagnac interferometers [21], pentaprism interferometers [111], and so on. It is worth noting that SLMs together with some interferometric arrangement have been proven to be a versatile tool to generate arbitrary non-uniformly polarized beams [23,44,49,57,93].

Two examples of NUTP beams generated by means of interferometers, one by amplitude division and the other by wavefront division, will be shown in this tutorial. The first one is based on a MZI with two different transparencies placed in its arms. This configuration has the advantage of being extremely versatile, because in principle, any NUTP can be realized in this way. The only limitation comes from the difficulty of producing transparencies with assigned complex transmission functions. Of course, holographic methods can be adopted to face the problem in the most general case, but interesting results can be obtained even with simple amplitude transmittances. In the second example, we use a Fresnel biprism to produce the two field components and let them superimpose. Dichroic polarizers are used to assign the right polarization to the two fields. The method is not very versatile, but the low versatility is compensated for by the extreme simplicity of the device, which can be used when different polarization states are required simultaneously across the beam section.

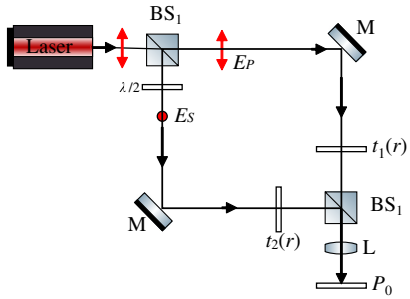

Fig. 7. MZI used to synthesize NUTP beams by means of amplitude transmittances, $t_i(r)$ with $i = 1, 2$. M's are mirrors, BS_i are beam splitters, $\lambda/2$ is a half-wave phase plate, and the subscripts s and p denote the polarization of the electric field (s perpendicular and p parallel to the incidence plane). L is a converging lens, which images the synthesized NUTP profile onto the plane P_0.

1. MZI and Amplitude Transmittances

Figure 7 shows the experimental setup. A collimated beam impinges onto one of the faces of a 50/50 non-polarizing beam splitter (BS_1). The input beam is linearly and uniformly polarized, parallel to the incidence plane. A half-wave plate with its fast axis at $\pi/4$ is inserted into one of the arms to rotate the polarization direction of the beam by $\pi/2$. Then, each of these beams with orthogonal linear polarization states impinges on an amplitude transmittance, $t_1(r)$ or $t_2(r)$, and they are eventually recombined by a second beam splitter (BS_2). At one of the exits of the interferometer, a converging lens (L) images the two fields obtained at the output of the transmittances onto the plane P_0. In our experiment, different apertures, having real transmittance with a super-Gaussian profile, are used as transparencies in the arms of the interferometer.

On assuming that the optical paths are identical (up to multiples of λ), and that mirrors and beam splitters do not introduce phase shift or tilt, the NUTP beam obtained at the output of the MZI can be described in the Jones formalism by the vector

$$\mathbf{E}_{\mathrm{MZ}}(\mathbf{r}) \propto \frac{E_0}{2}\begin{pmatrix} t_1(r) \\ t_2(r) \end{pmatrix} = \frac{E_0}{2}\begin{pmatrix} \exp\left[-\left(\frac{r}{w_1}\right)^{2n_1}\right] \\ \exp\left[-\left(\frac{r}{w_2}\right)^{2n_2}\right] \end{pmatrix}, \quad \textbf{(28)}$$

where E_0 is the amplitude of the incident field, supposed uniform within the super-Gaussian apertures. The shape of each aperture is determined by the width w_i and the order n_i, with $i = 1, 2$. The transmittance is flatter than the Gaussian function of the same width if $n_i = 1$, and becomes sharper and sharper for growing values of n_i. The typical polarization pattern expected in such conditions across the exit plane of the MZI is the one shown in Fig. 8(a), where only a transmittance with $n_2 = 2$ and $w_2 = 0.12$ mm is used (equivalent to let $w_1 \to \infty$). The states of polarization of this pattern are represented on the Poincaré sphere and cover a quarter of the equator, as can be seen in Fig. 8(b).

Polarization analysis is performed as for the previous examples. The bottom right part of Fig. 8 shows the behavior of the measured polarization direction of the exit field along a

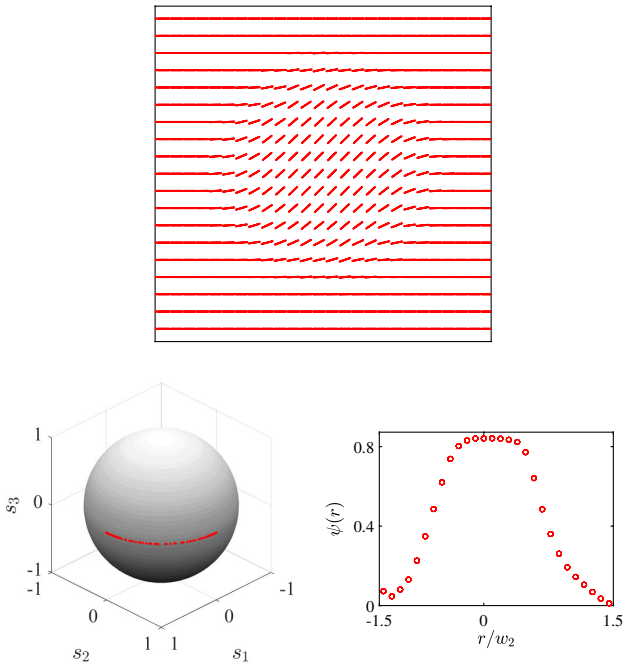

Fig. 8. Theoretical polarization pattern across the transverse section of a NUTP beam at the output of a MZI using only one super-Gaussian transmittance at one arm with $n_2 = 2$ and $w_2 = 0.12$ mm (top) and representation of the states of polarization on the Poincaré sphere (bottom left). Experimentally measured azimuth for the field obtained with the experimental setup in Fig. 7 (bottom right).

line passing through the center. For the experimental polarization pattern shown in Fig. 8, the global parameters are $\tilde{\mathcal{P}} = 1.01$, $\sigma_p^2 = 0.005$, $\rho_c = -0.10$, $\sigma_c^2 = 0.05$, $\rho_R = 0.502$, and $\rho_A = 0.498$, quite close to the theoretical ones: $\tilde{\mathcal{P}} = 1$, $\sigma_p^2 = 0$, $\rho_c = 0$, $\sigma_c^2 = 0$, $\rho_R = 1/2$, and $\rho_A = 1/2$. Due to the measurement errors of the irradiance, values of the local degree of polarization slightly greater than one could be obtained, which in turn could give rise to values greater than one for the experimental global degree of polarization. This is the case for the above result. It can be noted, however, that the experimental value is consistent with the expected one, $\tilde{\mathcal{P}} = 1$, if the uncertainty of the result is taken into account.

2. Fresnel Biprism

The interferometric system of the previous section is based on the division of the field amplitude. Other types of interferometers can be used for synthesizing NUTP beams, e.g., those based on the division of the field wavefront, as the Young's double-slit experiment [109,112–114]. Here, we show an example of a NUTP beam obtained by means of a formally equivalent system based on a Fresnel biprism [108].

The experimental setup is shown in Fig. 9. A linearly polarized laser beam is filtered and expanded by using a microscope objective, MO, a pinhole, PH, and a lens L_1. The collimated beam impinges onto a Fresnel biprism having refractive index n and acute angle α (supposed to be very small). Two dichroic polarizers, P_1 and P_2, with perpendicular transmission axes are placed in front of the top and the bottom prisms, respectively.

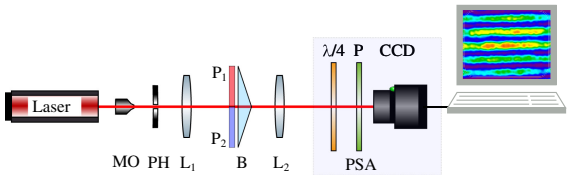

Fig. 9. Experimental setup. MO, microscope objective; PH, pinhole; L_1 and L_2, lenses; P_1 and P_2, polarizers; B, biprism; PSA, polarization state analyzer composed of a quarter-wave phase plate (λ/4), a polarizer (P), and a CCD camera.

The lens L_2 images onto the camera sensor the field present at the exit of the biprism. Polarization analysis is performed as for the previous examples.

Due to the difference in their propagation directions, the waves emerging from the two prisms reach a typical point of the output plane with different phases, so that the output beam turns out to be

$$\mathbf{E}_{\mathrm{BF}}(\mathbf{r}) \propto \begin{pmatrix} E_{0x}\, e^{ik\alpha(n-1)y} \\ E_{0y}\, e^{-ik\alpha(n-1)y} \end{pmatrix}, \tag{29}$$

where E_{0x} and E_{0y} are the input field components along x and y, respectively, k is the wave number in vacuum, and the losses at the interfaces have been neglected. The polarization state is seen to be dependent on the y coordinate. In particular it varies periodically, with period

$$\Lambda = \frac{\lambda}{2\alpha(n-1)}, \tag{30}$$

λ being the wavelength in vacuum.

The corresponding global parameters are $\tilde{\mathcal{P}} = 1$, $\sigma_p^2 = 0$, $\rho_c = 0, \sigma_c^2 = 0.5, \rho_r = 0.5$, and $\rho_a = 0.5$.

Figure 10, shows the theoretical (a) and experimental (b) polarization patterns for the case of linearly polarized input light with its azimuth at $\pi/4$. A BK7 biprism with $n = 1.515$, $\alpha = 1.5°$, and wavelength $\lambda = 632.8 \times 10^{-6}$ mm has been used. As expected, the polarization pattern is almost invariant along the x direction, while a periodic variation of the state of polarization along the y direction is observed. The produced field is the same as would be obtained using a polarization grating [80,97,115,116], but implementing the present approach can be much easier. It can be noted in Fig. 10 that the polarization states cover a meridian on the Poincaré sphere. Using a phase plate after the biprism, the polarization pattern can be modified and different maximum circles on the Poincaré sphere can be reached, depending on the orientation of the retardation of the plate.

The corresponding experimental global parameters are $\tilde{\mathcal{P}} = 0.93$, $\sigma_p^2 = 0.01$, $\rho_c = 0.01$, $\sigma_c^2 = 0.35$, $\rho_r = 0.54$, and $\rho_a = 0.46$.

C. Crystals

Anisotropic media, in particular uniaxial crystals, have been extensively used to produce phase wave plates. Plane parallel slabs of uniaxial crystals with their optical axes lying on the plane of the input face introduce a phase difference between ordinary and extraordinary waves due to the different propagation speeds

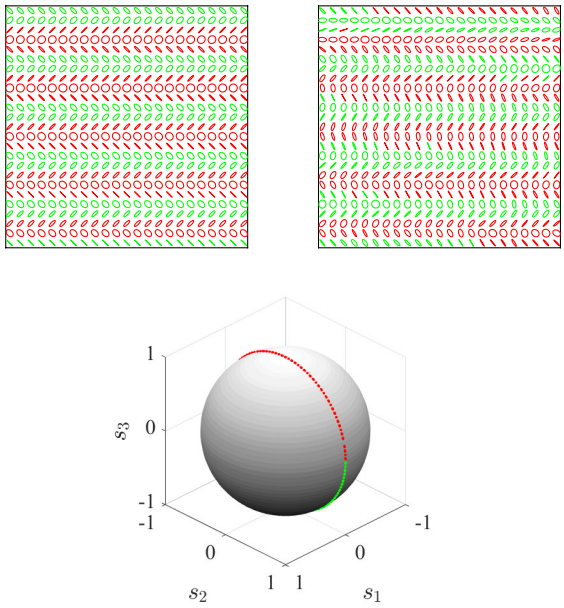

Fig. 10. Theoretical (upper left) and experimental (upper right) polarization pattern at the output of the biprism for input light linearly polarized with 45° azimuth with $\lambda = 632.8$ nm, $n = 1.515$, and $\alpha = 1.5°$. Red (green) ellipses denote right-handed (left-handed) polarization states. Poincaré sphere (bottom) where the states of polarization are represented.

of such components. Then, the polarization state of a uniformly polarized light is generally transformed into a different polarization state. By using different combinations of several wave phase plates, any state of polarization can be obtained from a uniformly polarized beam [117–119]. However, the phase delay is uniform across the whole phase wave plate, and if the input beam is uniformly polarized, the output beam is also uniformly polarized.

Conversely, by changing the orientation of the crystal axis or the incidence angle of the input beam, the polarization pattern at the exit of the crystal is, in general, no longer uniform. Using combinations of uniaxial crystals or biaxial crystals, a great variety of polarization patterns have been obtained [2,36,38,80,120–130]. Sometimes, these kinds of studies have been termed as interference of polarized light [2,120].

Here, two examples will be described in detail. The first one is based on the use of a plane parallel slab of a uniaxial crystal having its optic axis perpendicular to the input and output faces of the crystal [123,130]. The second one is based on a double wedge (DW), made up of two uniaxial crystal wedges with its optical axes parallel to the input and output faces but forming a $\pi/4$ angle between them [80,131].

1. Single Uniaxial Crystal

For the first case, we consider a parallelepiped made up of a uniaxial crystal with its axis along the propagation direction (z axis) of the incident beam, as shown in Fig. 11 (see references [70,123,130] for specific details). The input and output faces of the crystal are perpendicular to the crystal axis. Let us write the Jones vector of the input beam as

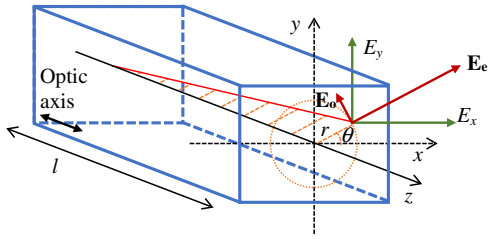

Fig. 11. Uniaxial crystal and field decomposition at the output face.

$$\mathbf{E}^{\text{in}} = \begin{pmatrix} E_{0x} \\ E_{0y}\exp(i\phi) \end{pmatrix}, \tag{31}$$

where ϕ is the phase difference between them. When the incident beam is focused onto the input face of the crystal, across the output plane the electric field can be decomposed into an ordinary wave (perpendicular to the principal plane) and an extraordinary wave (contained in the principal plane) [2]. They depend on the coordinates of the point across the exit face and can be written as [130]

$$\begin{aligned} \mathbf{E}_e(\mathbf{r}) &= [E_{0x}\cos\theta + E_{0y}\sin\theta\exp(i\phi)]\exp[ikn(\alpha)d_e]\,\mathbf{u}_r, \\ \mathbf{E}_o(\mathbf{r}) &= [-E_{0x}\sin\theta + E_{0y}\cos\theta\exp(i\phi)]\exp[ikn_o d_o]\,\mathbf{u}_\theta, \end{aligned} \tag{32}$$

where $\mathbf{u}_r$ and $\mathbf{u}_\theta$ are unitary vectors along the azimuthal and radial directions, respectively (see Fig. 11), n_o is the ordinary refractive index, and $n(\alpha)$ is the refractive index for the extraordinary wave whose propagation direction forms the angle α with respect to the optic axis. Losses at the input and output planes as well as refraction effects at the output face have been neglected. For small values of the angle α, both ordinary and extraordinary waves travel almost the same distance $d_e \simeq d_o \simeq d = \sqrt{l^2 + r^2}$, and $n(\alpha) \simeq n_e$, n_e being the extraordinary refractive index of the crystal [2,130].

It turns out [2,130] that the behavior of the uniaxial crystal, used as described above, can be described by the Jones matrix $\hat{T}_C(\mathbf{r}) = \{t_{ij}(\mathbf{r})\}$, with

$$\begin{aligned} t_{xx}(\mathbf{r}) &= \cos^2\theta\, e^{i\delta(r)/2} + \sin^2\theta\, e^{-i\delta(r)/2}, \\ t_{xy}(\mathbf{r}) &= i\sin 2\theta\,\sin[\delta(r)/2], \\ t_{yx}(\mathbf{r}) &= i\sin 2\theta\,\sin[\delta(r)/2], \\ t_{yy}(\mathbf{r}) &= \cos^2\theta\, e^{-i\delta(r)/2} + \sin^2\theta\, e^{i\delta(r)/2}, \end{aligned} \tag{33}$$

where the phase difference $\delta(r)$ has been introduced as

$$\delta(r) \simeq k[n(\alpha) - n_o]d \simeq k(n_e - n_o)\frac{r^2}{d}, \tag{34}$$

and an unessential overall phase term has been omitted. It can be noted that such a Jones matrix corresponds to that of a spatially varying phase wave plate having retardance $\delta(r)$ and fast axis rotated by θ with respect to the x axis [4].

Figure 12 shows the polarization pattern that would be obtained at the exit of the crystal for the case of a He–Ne laser input beam linearly polarized along y and a calcite crystal

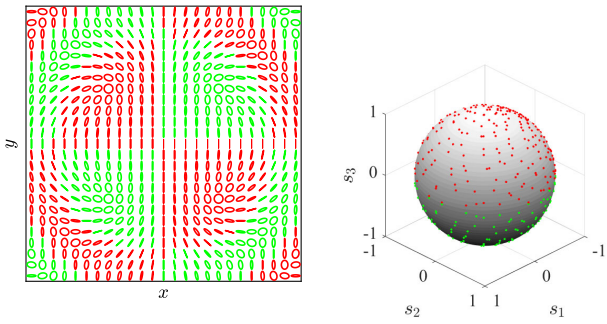

Fig. 12. Theoretical polarization pattern at the output of the calcite crystal for input light linearly polarized with $\pi/2$ azimuth and $\lambda = 632.8$ nm (left) and Poincaré sphere with dots corresponding to the ellipses of polarization shown in the polarization pattern (right). Red (green) ellipses and dots denote right-handed (left-handed) polarization states.

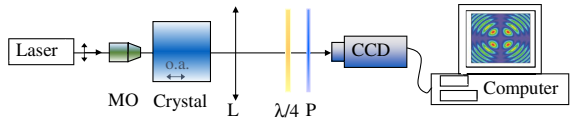

Fig. 13. Experimental setup for synthesizing a NUTP beam by means of a calcite crystal. MO is a microscope objective, L a lens, $\lambda/4$ a quarter-wave phase plate, and P a dichroic polarizer.

20 mm thick. For this kind of beam, the corresponding theoretical global parameters are $\tilde{\mathcal{P}} = 1$, $\sigma_p^2 = 0$, $\rho_c = 0$, $\sigma_c^2 = 0.25$, $\rho_r = 0.5$, and $\rho_a = 0.5$.

It has been recently shown that such a pattern contains all possible totally polarized states [130], so that the output beam is actually a FPB.

Figure 13 shows an experimental setup to experimentally synthesize a FPB by using a uniaxial crystal [130]. A laser beam is linearly polarized along the y direction by means of the linear polarizer P_1. The microscope objective, MO, focuses the beam at the input face of a uniaxial crystal with its optic axis oriented along the z axis. The polarization analysis of the field exiting the crystal is performed as for the previous examples.

Figure 14 shows the experimentally measured polarization pattern across the beam section in the same region as for Fig. 12. An excellent agreement between the theoretical and experimental results can be observed.

From the experimental polarization pattern, the corresponding global parameters are $\tilde{\mathcal{P}} = 1.03$, $\sigma_p^2 = 0.08$, $\rho_c = 0.04$, $\sigma_c^2 = 0.22$, $\rho_r = 0.51$, and $\rho_a = 0.49$.

2. Double Wedge

A slightly more complex optical system uses a DW. This is a device typically used to produce beams that present fast spatial variation of the state of polarization across their transverse section. In such a way, when the Stokes parameters are measured with low enough spatial resolution, the field appears as being unpolarized. Therefore, the DW is often used as a spatial depolarizer. It should be clear, however, that if the incident field is

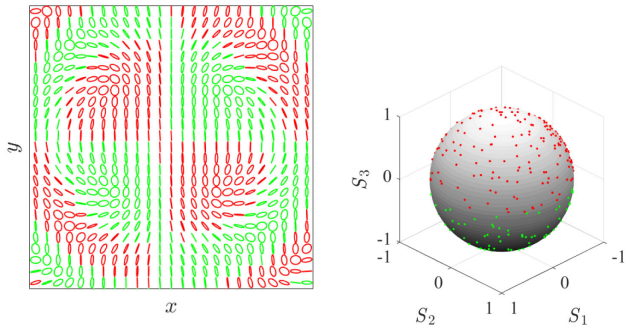

Fig. 14. Experimental polarization pattern at the output of the calcite crystal for input light linearly polarized with $\pi/2$ azimuth and $\lambda = 632.8$ nm (left), and Poincaré sphere with dots corresponding to the ellipses of polarization shown in the polarization pattern (right). Red (green) ellipses and dots denote right-handed (left-handed) polarization states.

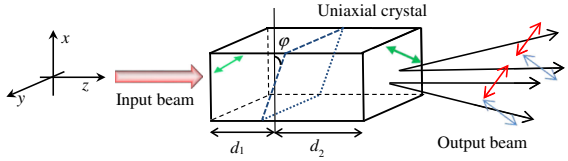

Fig. 15. Scheme of a double-wedge anisotropic crystal. Green arrows denote the orientation of the optic axis of each part of the double wedge. Both optic axes are perpendicular to the z axis, and the angle between them is $\pi/4$. Red and blue arrows denote the linear polarization directions of each exiting beam. The wedge angle is φ.

totally polarized, the same happens for the output field, but the latter is a NUTP beam.

A DW consists of two birefringent wedges with the same angle wedge φ (typically a few degrees), joined to form a parallelepiped (see Fig. 15). The optic axis of the first wedge is, for example, along the y direction. The second one has its optic axis parallel to the bisector of the x and y axes. The reader should not confuse a DW with a Wollaston prism, which presents a similar geometry but for which the optic axes of the two crystals are mutually orthogonal.

If a plane wave impinges perpendicularly to the input face of the DW with arbitrary state of polarization, e.g., linearly polarized with $\pi/4$ azimuth, four field components can be identified at the output [80,131–134]: two plane waves propagating along the same direction as the incident wave but with different phases and orthogonal polarization, and two plane waves, also having mutually orthogonal polarization, that propagate along slightly tilted directions. The effect of the superposition of such waves is a modulation of the state of polarization of the field across the exit plane of the device.

Neglecting the losses due to reflections at the interfaces and the small differences between the transmission coefficients for ordinary and extraordinary waves or between the parallel and perpendicular components at the exit face, and assuming that the propagation direction of all components is essentially along the z axis, the Jones matrix $\hat{T}_{\mathrm{DW}}(\mathbf{r}) = (t_{ij}(\mathbf{r}))$ of the DW can be evaluated as [80,131]

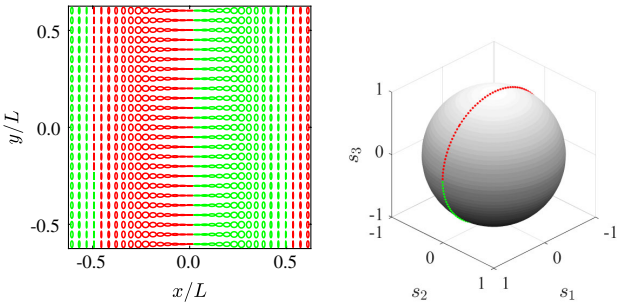

Fig. 16. Polarization pattern at the exit of a DW when a linearly polarized light along y axis inputs in it (left) and Poincaré sphere where the states of polarization are represented (right). Red (green) ellipses and dots denote right-handed (left-handed) polarization states.

$$t_{xx}(\mathbf{r}) = \frac{1}{2}\left[1 + \exp\left(\mathrm{i}\delta_2(x)\right)\right],$$

$$t_{xy}(\mathbf{r}) = \frac{1}{2}\left[1 + \exp\left(\mathrm{i}\delta_2(x)\right)\right]\exp\left(\mathrm{i}\delta_1(x)\right),$$

$$t_{yx}(\mathbf{r}) = \frac{1}{2}\left[-1 + \exp\left(\mathrm{i}\delta_2(x)\right)\right],$$

$$t_{yy}(\mathbf{r}) = \frac{1}{2}\left[-1 + \exp\left(\mathrm{i}\delta_2(x)\right)\right]\exp\left(\mathrm{i}\delta_1(x)\right). \quad (35)$$

As is evident from Eq. (35), the geometry of the DW yields a Jones matrix that depends only on the x coordinate, so that the same polarization state is expected at all points along lines with $x =$ constant across the output plane. For any uniformly polarized input field, the output beam shows a periodic variation of the polarization state along x direction, with period

$$L = \frac{\lambda}{|n_e(\lambda) - n_o(\lambda)|\tan\varphi}, \quad (36)$$

similar to that obtained with polarization gratings but presenting, with respect to the latter, advantages in terms of ease of implementation and reduction of losses.

The polarization distribution pattern is represented in Fig. 16 for a He–Ne laser wavelength and a quartz DW with $\varphi = 2°$. The results are shown in Fig. 16, and for this case, the period turns out to be $L \simeq 2.0$ mm. The global parameters corresponding to this particular beam computed over an integer number of periods are $\tilde{\mathcal{P}} = 1$, $\sigma_p^2 = 0$, $\rho_c = 0$, $\sigma_c^2 = 0.5$, $\rho_r = 0.5$, and $\rho_a = 0.5$.

The technique has been implemented, and the experimental setup shown in Fig. 17 has been arranged. A He–Ne laser beam, polarized along the y direction, was magnified by a microscope objective and a lens, and entered the DW (DPU25 from Thorlabs, in this experiment). At the output, a commercial polarimeter (PAX5710VIS from Thorlabs) with a small pinhole (50 μm diameter) attached at its entrance was used to determine the state of polarization of the beam in a small area. This polarimeter was mounted on an x micropositioner so that the state of polarization could be measured across the beam profile.

Figure 18(a) shows the measured Stokes parameters (normalized) where a sinusoidal variation is observed for both s_1 and s_3, while s_2 is close to zero. In a whole period, the state of

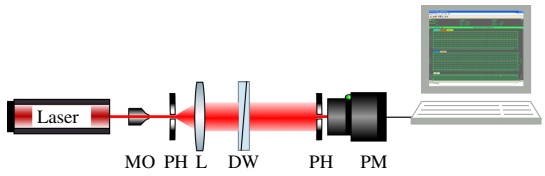

Fig. 17. Experimental setup to generate a NUTP beam by means of a DW.

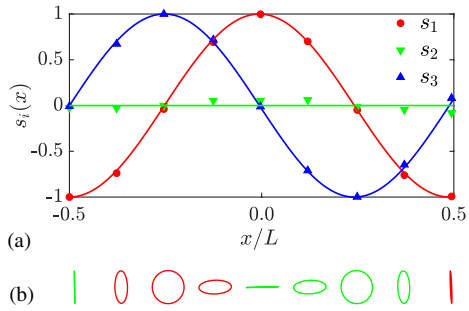

Fig. 18. (a) Measured Stokes parameters at the exit of a DW along the x direction and (b) the corresponding ellipse of polarization. Red (green) ellipses denote right-handed (left-handed) polarization states.

polarization covers the meridian on the Poincaré sphere that passes on the vertical and horizontal states of polarization.

5. SUMMARY

In many cases, a single state of polarization is found across the transverse section of a beam, and one polarization ellipse is enough to represent its polarization. Often, however, the polarization state of a beam varies from point to point, giving rise to NUTP beams. The latter present many interesting characteristics and numerous applications, so they have attracted great attention among the scientific community. This tutorial intends to introduce this subject, starting from the basic tools to describe and represent the polarization of light. Some local and global parameters for characterizing NUTP beams have been introduced. Furthermore, some simple experimental techniques aimed at producing NUTP beams, which can be easily implemented in any optics laboratory, have been presented. It is expected that this tutorial will serve as incentive and help for newcomers in the field who want to get started on this topic in a simple way.

Funding. Ministerio de Economía y Competitividad (FIS2016-75147).

Acknowledgment. We gratefully acknowledge valuable discussions and suggestions from Professor Franco Gori.

REFERENCES

1. W. A. Shurcliff, *Polarized Light* (Harvard University, 1962).
2. M. Born and E. Wolf, *Principles of Optics*, 6th (corrected) ed. (Cambridge University, 1980).

3. C. Brosseau, *Fundamentals of Polarized Light: A Statistical Optics Approach*, 1st ed. (Wiley, 1998).
4. D. H. Goldstein, *Polarized Light*, 2nd (revised and expanded) ed. (Marcel Dekker, Inc., 2003).
5. Q. Zhan, *Vectorial Optical Fields* (World Scientific, 2014).
6. E. J. Galvez, *Light Beams with Spatially Variable Polarization* (Wiley, 2015), Chap. 3, pp. 61–76.
7. J. J. Gil and R. Ossikovski, *Polarized Light and the Mueller Matrix Approach* (CRC Press/Taylor & Francis Group, 2016).
8. R. Chipman, W. Lam, and G. Young, *Polarized Light and Optical Systems, Optical Sciences and Applications of Light* (CRC Press, 2018).
9. T. Bauer, P. Banzer, E. Karimi, S. Orlov, A. Rubano, L. Marrucci, E. Santamato, R. W. Boyd, and G. Leuchs, "Observation of optical polarization Möbius strips," Science **347**, 964–966 (2015).
10. T. Wakayama, T. Higashiguchi, K. Sakaue, M. Washio, and Y. Otani, "Demonstration of a terahertz pure vector beam by tailoring geometric phase," Sci. Rep. **8**, 8690 (2018).
11. N. Bhebhe, P. A. C. Williams, C. Rosales-Guzmán, V. Rodriguez-Fajardo, and A. Forbes, "A vector holographic optical trap," Sci. Rep. **8**, 17387 (2018).
12. H. Larocque, D. Sugic, D. Mortimer, A. Taylor, R. Fickler, R. Boyd, M. Dennis, and E. Karimi, "Reconstructing the topology of optical polarization knots," Nat. Phys. **36**, 4104–4106 (2018).
13. N. A. Rubin, G. D'Aversa, P. Chevalier, Z. Shi, W. T. Chen, and F. Capasso, "Matrix Fourier optics enables a compact full-Stokes polarization camera," Science **365**, eaax1839 (2019).
14. Y. Mushiake, K. Matsumura, and N. Nakajima, "Generation of radially polarized optical beam mode by laser oscillation," Proc. IEEE **60**, 1107–1109 (1972).
15. S. C. Tidwell, D. H. Ford, and W. D. Kimura, "Generating radially polarized beams interferometrically," Appl. Opt. **29**, 2234–2239 (1990).
16. T. Erdogan, O. King, G. W. Wicks, D. G. Hall, E. H. Anderson, and M. J. Rooks, "Concentric-circle-grating, surface-emitting semiconductor lasers," Opt. Photon. News **3**(12), 41 (1992).
17. F. Gori, "Polarization basis for vortex beams," J. Opt. Soc. Am. A **18**, 1612–1617 (2001).
18. I. Freund, "Polarization flowers," Opt. Commun. **199**, 47–63 (2001).
19. M. Dennis, "Polarization singularities in paraxial vector fields: morphology and statistics," Opt. Commun. **213**, 201–221 (2002).
20. O. Angelsky, A. Mokhun, I. Mokhun, and M. Soskin, "The relationship between topological characteristics of component vortices and polarization singularities," Opt. Commun. **207**, 57–65 (2002).
21. V. G. Niziev, R. S. Chang, and A. V. Nesterov, "Generation of inhomogeneously polarized laser beams by use of a Sagnac interferometer," Appl. Opt. **45**, 8393–8399 (2006).
22. L. Marrucci, C. Manzo, and D. Paparo, "Optical spin-to-orbital angular momentum conversion in inhomogeneous anisotropic media," Phys. Rev. Lett. **96**, 163905 (2006).
23. C. Maurer, A. Jesacher, S. Fürhapter, S. Bernet, and M. Ritsch-Marte, "Tailoring of arbitrary optical vector beams," New J. Phys. **9**, 78 (2007).
24. R. Martínez-Herrero and P. M. Mejías, "Propagation of light fields with radial or azimuthal polarization distribution at a transverse plane," Opt. Express **16**, 9021–9033 (2008).
25. Q. Zhan, "Cylindrical vector beams: from mathematical concepts to applications," Adv. Opt. Photon. **1**, 1–57 (2009).
26. V. Ramírez-Sánchez, G. Piquero, and M. Santarsiero, "Generation and characterization of spirally polarized fields," J. Opt. A **11**, 085708 (2009).
27. V. Ramírez-Sánchez, G. Piquero, and M. Santarsiero, "Synthesis and characterization of partially coherent beams with propagation-invariant transverse polarization pattern," Opt. Commun. **283**, 4484–4489 (2010).
28. T. G. Brown, *Unconventional Polarization States: Beam Propagation, Focusing, and Imaging* (Elsevier, 2011), vol. **56** of Progress in Optics, Chap. 2, pp. 81–129.
29. G. Milione, H. I. Sztul, D. A. Nolan, and R. R. Alfano, "Higher-order Poincaré sphere, Stokes parameters, and the angular momentum of light," Phys. Rev. Lett. **107**, 053601 (2011).
30. L. Marrucci, E. Karimi, S. Slussarenko, B. Piccirillo, E. Santamato, E. Nagali, and F. Sciarrino, "Spin-to-orbital conversion of the angular momentum of light and its classical and quantum applications," J. Opt. **13**, 064001 (2011).
31. G. Milione, S. Evans, D. A. Nolan, and R. R. Alfano, "Higher order Pancharatnam-Berry phase and the angular momentum of light," Phys. Rev. Lett. **108**, 190401 (2012).
32. J. C. G. de Sande, G. Piquero, and C. Teijeiro, "Polarization changes at Lyot depolarizer output for different types of input beams," J. Opt. Soc. Am. A: **29**, 278–284 (2012).
33. T. G. Brown and A. M. Beckley, "Stress engineering and the applications of inhomogeneously polarized optical fields," Front. Optoelectron. **6**, 89–96 (2013).
34. S. Vyas, Y. Kozawa, and S. Sato, "Polarization singularities in superposition of vector beams," Opt. Express **21**, 8972–8986 (2013).
35. F. Cardano, E. Karimi, L. Marrucci, C. de Lisio, and E. Santamato, "Generation and dynamics of optical beams with polarization singularities," Opt. Express **21**, 8815–8820 (2013).
36. V. G. Shvedov, C. Hnatovsky, N. Shostka, and W. Krolikowski, "Generation of vector bottle beams with a uniaxial crystal," J. Opt. Soc. Am. B **30**, 1–6 (2013).
37. X. Zheng, A. Lizana, A. Peinado, C. Ramírez, J. L. Martínez, A. Márquez, I. Moreno, and J. Campos, "Compact LCOS–SLM based polarization pattern beam generator," J. Lightwave Technol. **33**, 2047–2055 (2015).
38. A. Turpin, Y. V. Loiko, A. Peinado, A. Lizana, T. K. Kalkandjiev, J. Campos, and J. Mompart, "Polarization tailored novel vector beams based on conical refraction," Opt. Express **23**, 5704–5715 (2015).
39. W. Zhu, V. Shvedov, W. She, and W. Krolikowski, "Transverse spin angular momentum of tightly focused full Poincaré beams," Opt. Express **23**, 34029–34041 (2015).
40. M. McLaren, T. Konrad, and A. Forbes, "Measuring the nonseparability of vector vortex beams," Phys. Rev. A **92**, 023833 (2015).
41. B. Ndagano, H. Sroor, M. McLaren, C. Rosales-Guzmán, and A. Forbes, "Beam quality measure for vector beams," Opt. Lett. **41**, 3407–3410 (2016).
42. J. A. Davis, I. Moreno, K. Badham, M. M. Sánchez-López, and D. M. Cottrell, "Nondiffracting vector beams where the charge and the polarization state vary with propagation distance," Opt. Lett. **41**, 2270–2273 (2016).
43. D. Naidoo, F. S. Roux, A. Dudley, I. Litvin, B. Piccirillo, L. Marrucci, and A. Forbes, "Controlled generation of higher-order Poincaré sphere beams from a laser," Nat. Photonics **10**, 327–332 (2016).
44. H. Rubinsztein-Dunlop, A. Forbes, M. V. Berry, M. R. Dennis, D. L. Andrews, M. Mansuripur, C. Denz, C. Alpmann, P. Banzer, T. Bauer, E. Karimi, L. Marrucci, M. Padgett, M. Ritsch-Marte, N. M. Litchinitser, N. P. Bigelow, C. Rosales-Guzmán, A. Belmonte, J. P. Torres, T. W. Neely, M. Baker, R. Gordon, A. B. Stilgoe, J. Romero, A. G. White, R. Fickler, A. E. Willner, G. Xie, B. McMorran, and A. M. Weiner, "Roadmap on structured light," J. Opt. **19**, 013001 (2017).
45. C. H. Krishna and S. Roy, "Generation of inhomogeneously polarized vector vortex modes in few mode optical fiber," Opt. Quantum Electron. **51**, 41 (2019).
46. A. M. Beckley, T. G. Brown, and M. A. Alonso, "Full Poincaré beams," Opt. Express **18**, 10777–10785 (2010).
47. W. Han, W. Cheng, and Q. Zhan, "Flattop focusing with full Poincaré beams under low numerical aperture illumination," Opt. Lett. **36**, 1605–1607 (2011).
48. E. J. Galvez, S. Khadka, W. H. Schubert, and S. Nomoto, "Poincaré-beam patterns produced by nonseparable superpositions of Laguerre-Gauss and polarization modes of light," Appl. Opt. **51**, 2925–2934 (2012).
49. S. Chen, X. Zhou, Y. Liu, X. Ling, H. Luo, and S. Wen, "Generation of arbitrary cylindrical vector beams on the higher order Poincaré sphere," Opt. Lett. **39**, 5274–5276 (2014).
50. C. Wei, D. Wu, C. Liang, F. Wang, and Y. Cai, "Experimental verification of significant reduction of turbulence-induced scintillation in a full Poincaré beam," Opt. Express **23**, 24331–24341 (2015).
51. D. Colas, L. Dominici, S. Donati, A. A. Pervishko, T. C. Liew, I. A. Shelykh, D. Ballarini, M. de Giorgi, A. Bramati, G. Gigli, E. del Valle, F. P. Laussy, A. V. Kavolin, and D. Sanvito, "Polarization shaping of

Poincaré beams by polariton oscillations," Light Sci. Appl. **4**, e350 (2015).
52. I. S. Moreno, J. A. Davis, K. D'Nelly, and D. B. Allison, "Transmission and phase measurements for polarization eigenvectors in twisted-nematic liquid crystal spatial light modulators," Opt. Eng. **37**, 144–3052 (1998).
53. V. G. Niziev and A. V. Nesterov, "Influence of beam polarization on laser cutting efficiency," J. Phys. D **32**, 1455–1461 (1999).
54. L. Novotny, M. R. Beversluis, K. S. Youngworth, and T. G. Brown, "Longitudinal field modes probed by single molecules," Phys. Rev. Lett. **86**, 5251–5254 (2001).
55. R. Dorn, S. Quabis, and G. Leuchs, "Sharper focus for a radially polarized light beam," Phys. Rev. Lett. **91**, 233901 (2003).
56. Q. Zhan, "Trapping metallic Rayleigh particles with radial polarization," Opt. Express **12**, 3377–3382 (2004).
57. X.-L. Wang, J. Ding, W.-J. Ni, C.-S. Guo, and H.-T. Wang, "Generation of arbitrary vector beams with a spatial light modulator and a common path interferometric arrangement," Opt. Lett. **32**, 3549–3551 (2007).
58. K. J. Moh, X.-C. Yuan, J. Bu, S. W. Zhu, and B. Z. Gao, "Radial polarization induced surface plasmon virtual probe for two-photon fluorescence microscopy," Opt. Lett. **34**, 971–973 (2009).
59. W. Chen and Q. Zhan, "Diffraction limited focusing with controllable arbitrary three-dimensional polarization," J. Opt. **12**, 045707 (2010).
60. F. Kenny, D. Lara, O. G. Rodríguez-Herrera, and C. Dainty, "Complete polarization and phase control for focus-shaping in high-NA microscopy," Opt. Express **20**, 14015–14029 (2012).
61. I. Moreno, J. A. Davis, T. M. Hernandez, D. M. Cottrell, and D. Sand, "Complete polarization control of light from a liquid crystal spatial light modulator," Opt. Express **20**, 364–376 (2012).
62. K. Lou, S.-X. Qian, Z.-C. Ren, C. Tu, Y. Li, and H.-T. Wang, "Femtosecond laser processing by using patterned vector optical fields," Sci. Rep. **3**, 2281 (2013).
63. J. C. G. de Sande, M. Santarsiero, and G. Piquero, "Spirally polarized beams for polarimetry measurements of deterministic and homogeneous samples," Opt. Laser Eng. **91**, 97–105 (2017).
64. H. Zhang, J. Li, K. Cheng, M. Duan, and Z. Feng, "Trapping two types of particles using a focused partially coherent circular edge dislocations beam," Opt. Laser Technol. **97**, 191–197 (2017).
65. J. C. G. de Sande, G. Piquero, and M. Santarsiero, "Polarimetry with non uniformly polarized beams," in *2nd Joensuu Conference on Coherence and Random Polarization. Trends in Electromagnetic Coherence* (2018), pp. 76–77.
66. J. Chen, C. Wan, and Q. Zhan, "Vectorial optical fields: recent advances and future prospects," Sci. Bull. **63**(1), 54–74 (2018).
67. A. Martnez, "Polarimetry enabled by nanophotonics," Science **362**, 750–751 (2018).
68. J. C. G. de Sande, G. Piquero, and M. Santarsiero, "Polarimetry with azimuthally polarized light," Opt. Commun. **410**, 961–965 (2018).
69. J. Zeng, R. Lin, X. Liu, C. Zhao, and Y. Cai, "Review on partially coherent vortex beams," Front. Optoelectron. **12**, 229–248 (2019).
70. J. C. Suárez-Bermejo, J. C. G. de Sande, M. Santarsiero, and G. Piquero, "Mueller matrix polarimetry using full Poincaré beams," Opt. Laser Eng. **122**, 134–141 (2019).
71. C. J. R. Sheppard, "Jones and Stokes parameters for polarization in three dimensions," Phys. Rev. A **90**, 023809 (2014).
72. A. T. Friberg and T. Setälä, "Electromagnetic theory of optical coherence (invited)," J. Opt. Soc. Am. A **33**, 2431–2442 (2016).
73. K. Tekce, E. Otte, and C. Denz, "Optical singularities and Möebius strip arrays in tailored non-paraxial light fields," Opt. Express **27**, 29685–29696 (2019).
74. R. Martínez-Herrero, P. M. Mejías, and G. Piquero, *Characterization of Partially Polarized Light Fields*, Springer Series in Optical Science (Springer, 2009).
75. K. S. Youngworth and T. G. Brown, "Focusing of high numerical aperture cylindrical-vector beams," Opt. Express **7**, 77–87 (2000).
76. A. Lapucci and M. Ciofini, "Polarization state modifications in the propagation of high azimuthal order annular beams," Opt. Express **9**, 603–609 (2001).
77. Q. Zhan and J. R. Leger, "Focus shaping using cylindrical vector beams," Opt. Express **10**, 324–331 (2002).
78. J. Tervo, "Azimuthal polarization and partial coherence," J. Opt. Soc. Am. A **20**, 1974–1980 (2003).
79. R. Borghi and M. Santarsiero, "Nonparaxial propagation of spirally polarized optical beams," J. Opt. Soc. Am. A **21**, 2029–2037 (2004).
80. J. C. G. de Sande, M. Santarsiero, G. Piquero, and F. Gori, "Longitudinal polarization periodicity of unpolarized light passing through a double wedge depolarizer," Opt. Express **20**, 27348–27360 (2012).
81. R. Martínez-Herrero and F. Prado, "Polarization evolution of radially polarized partially coherent vortex fields: role of Gouy phase of Laguerre–Gauss beams," Opt. Express **23**, 5043–5051 (2015).
82. E. Wolf, *Introduction to the Theory of Coherence and Polarization of Light* (Cambridge University, 2007).
83. F. Gori, M. Santarsiero, S. Vicalvi, R. Borghi, and G. Guattari, "Beam coherence-polarization matrix," Pure Appl. Opt. **7**, 941 (1998).
84. E. Wolf, "Can a light beam be considered to be the sum of a completely polarized and a completely unpolarized beam?" Opt. Lett. **33**, 642–644 (2008).
85. J. Tervo and J. Turunen, "Comment on 'Can a light beam be considered to be the sum of a completely polarized and a completely unpolarized beam?'" Opt. Lett. **34**, 1001 (2009).
86. V. Ramírez-Sánchez and G. Piquero, "The beam quality parameter of spirally polarized beams," J. Opt. A **10**, 125004 (2008).
87. G. Piquero, J. M. Movilla, P. M. Mejías, and R. Martínez-Herrero, "Degree of polarization of non-uniformly partially polarized beams: a proposal," Opt. Quantum Electron. **31**, 223–226 (1999).
88. P. M. Mejías, R. Martínez-Herrero, G. Piquero, and J. M. Movilla, "Parametric characterization of the spatial structure of non-uniformly polarized laser beams," Prog. Quantum Electron. **26**, 65–130 (2002).
89. R. Martínez-Herrero, P. Mejías, and G. Piquero, "Overall parameters for the characterization of non-uniformly totally polarized beams," Opt. Commun. **265**, 6–10 (2006).
90. R. Martínez-Herrero, P. Mejías, G. Piquero, and V. Ramírez-Sánchez, "Global parameters for characterizing the radial and azimuthal polarization content of totally polarized beams," Opt. Commun. **281**, 1976–1980 (2008).
91. Y. Ma and R. Wu, "Characterizing polarization properties of radially polarized beams," Opt. Rev. **21**, 4–8 (2014).
92. T. Alieva, J. A. Rodrigo, A. Cámara, and E. Abramochkin, "Partially coherent stable and spiral beams," J. Opt. Soc. Am. A **30**, 2237–2243 (2013).
93. D. Maluenda, I. Juvells, R. Martínez-Herrero, and A. Carnicer, "Reconfigurable beams with arbitrary polarization and shape distributions at a given plane," Opt. Express **21**, 5432–5439 (2013).
94. B. Pérez-García, C. López-Mariscal, R. I. Hernández-Aranda, and J. C. Gutiérrez-Vega, "On-demand tailored vector beams," Appl. Opt. **56**, 6967–6972 (2017).
95. C. Rosales-Guzmán, B. Ndagano, and A. Forbes, "A review of complex vector light fields and their applications," J. Opt. **20**, 123001 (2018).
96. V. Arrizón, E. Tepichin, M. Ortiz-Gutierrez, and A. Lohmann, "Fresnel diffraction at 1/4 of the Talbot distance of an anisotropic grating," Opt. Commun. **127**, 171–175 (1996).
97. F. Gori, "Measuring Stokes parameters by means of a polarization grating," Opt. Lett. **24**, 584–586 (1999).
98. J. Tervo and J. Turunen, "Transverse and longitudinal periodicities in fields produced by polarization gratings," Opt. Commun. **190**, 51–57 (2001).
99. G. Piquero, R. Borghi, and M. Santarsiero, "Gaussian Schell-model beams propagating through polarization gratings," J. Opt. Soc. Am. A **18**, 1399–1405 (2001).
100. G. Piquero, R. Borghi, A. Mondello, and M. Santarsiero, "Far field of beams generated by quasi-homogeneous sources passing through polarization gratings," Opt. Commun. **195**, 339–350 (2001).
101. Z. Bomzon, G. Biener, V. Kleiner, and E. Hasman, "Radially and azimuthally polarized beams generated by space-variant dielectric subwavelength gratings," Opt. Lett. **27**, 285–287 (2002).
102. A. Niv, G. Biener, V. Kleiner, and E. Hasman, "Formation of linearly polarized light with axial symmetry by use of space-variant subwavelength gratings," Opt. Lett. **28**, 510–512 (2003).

103. S. N. Khonina and S. V. Karpeev, "Grating-based optical scheme for the universal generation of inhomogeneously polarized laser beams," Appl. Opt. **49**, 1734–1738 (2010).
104. Z. Bomzon, G. Biener, V. Kleiner, and E. Hasman, "Real-time analysis of partially polarized light with a space-variant subwavelength dielectric grating," Opt. Lett. **27**, 188–190 (2002).
105. G. Biener, A. Niv, V. Kleiner, and E. Hasman, "Computer-generated infrared depolarizer using space-variant subwavelength dielectric gratings," Opt. Lett. **28**, 1400–1402 (2003).
106. Z. Bomzon, G. Biener, V. Kleiner, and E. Hasman, "Space-variant Pancharatnam–Berry phase optical elements with computer-generated subwavelength gratings," Opt. Lett. **27**, 1141–1143 (2002).
107. M. Stalder and M. Schadt, "Linearly polarized light with axial symmetry generated by liquid-crystal polarization converters," Opt. Lett. **21**, 1948–1950 (1996).
108. G. Piquero, I. Marcos-Muñoz, and J. C. G. de Sande, "Simple undergraduate experiment for synthesizing and analyzing non-uniformly polarized beams by means of a Fresnel biprism," Am. J. Phys. **87**, 208–213 (2019).
109. Y. Li, X.-L. Wang, H. Zhao, L.-J. Kong, K. Lou, B. Gu, C. Tu, and H.-T. Wang, "Young's two-slit interference of vector light fields," Opt. Lett. **37**, 1790–1792 (2012).
110. K. C. Toussaint, S. Park, J. E. Jureller, and N. F. Scherer, "Generation of optical vector beams with a diffractive optical element interferometer," Opt. Lett. **30**, 2846–2848 (2005).
111. C.-Y. Han, R.-S. Chang, and H.-F. Chen, "Solid-state interferometry of a pentaprism for generating cylindrical vector beam," Opt. Rev. **20**, 189–192 (2013).
112. J. Qi, W. Wang, X. Li, X. Wang, W. Sun, J. Liao, and Y. Nie, "Double-slit interference of radially polarized vortex beams," Opt. Eng. **53**, 044107 (2014).
113. O. Arteaga, R. Ossikovski, E. Kuntman, M. A. Kuntman, A. Canillas, and E. Garcia-Caurel, "Mueller matrix polarimetry on a Young's double-slit experiment analog," Opt. Lett. **42**, 3900–3903 (2017).
114. A. Hannonen, H. Partanen, J. Tervo, T. Setälä, and A. T. Friberg, "Pancharatnam-Berry phase in electromagnetic double-pinhole interference," Phys. Rev. A **99**, 053826 (2019).
115. Y. Gorodetski, G. Biener, A. Niv, V. Kleiner, and E. Hasman, "Space-variant polarization manipulation for far-field polarimetry by use of subwavelength dielectric gratings," Opt. Lett. **30**, 2245–2247 (2005).
116. M. Santarsiero, J. C. G. de Sande, G. Piquero, and F. Gori, "Coherence-polarization properties of fields radiated from transversely periodic electromagnetic sources," J. Opt. **15**, 055701 (2013).
117. R. Simon and N. Mukunda, "Universal SU(2) gadget for polarization optics," Phys. Lett. A **138**, 474–480 (1989).
118. R. Simon and N. Mukunda, "Minimal three-component SU(2) gadget for polarization optics," Phys. Lett. A **143**, 165–169 (1990).
119. V. Bagini, R. Borghi, F. Gori, M. Santarsiero, F. Frezza, G. Schettini, and G. Spagnolo, "The Simon–Mukunda polarization gadget," Eur. J. Phys. **17**, 279–284 (1996).
120. P. H. Äyräs, A. T. Friberg, M. A. J. Kaivola, and M. M. Salomaa, "Conoscopic interferometry of surface-acoustic-wave substrate crystals," Appl. Opt. **38**, 5399–5407 (1999).
121. A. Ciattoni, G. Cincotti, and C. Palma, "Ordinary and extraordinary beams characterization in uniaxially anisotropic crystals," Opt. Commun. **195**, 55–61 (2001).
122. A. Ciattoni, G. Cincotti, and C. Palma, "Circularly polarized beams and vortex generation in uniaxial media," J. Opt. Soc. Am. A **20**, 163–171 (2003).
123. G. Piquero and J. Vargas-Balbuena, "Non-uniformly polarized beams across their transverse profiles: an introductory study for undergraduate optics courses," Eur. J. Phys. **25**, 793–800 (2004).
124. A. Volyar, V. Shvedov, T. Fadeyeva, A. S. Desyatnikov, D. N. Neshev, W. Krolikowski, and Y. S. Kivshar, "Generation of single-charge optical vortices with an uniaxial crystal," Opt. Express **14**, 3724–3729 (2006).
125. M. Erdélyi and G. Gajdátsy, "Radial and azimuthal polarizer by means of a birefringent plate," J. Opt. A **10**, 055007 (2008).
126. T. A. Fadeyeva, V. G. Shvedov, Y. V. Izdebskaya, A. V. Volyar, E. Brasselet, D. N. Neshev, A. S. Desyatnikov, W. Krolikowski, and Y. S. Kivshar, "Spatially engineered polarization states and optical vortices in uniaxial crystals," Opt. Express **18**, 10848–10863 (2010).
127. N. Khilo, T. S. Al-Saud, S. H. Al-Khowaiter, M. K. Al-Muhanna, S. Solonevich, N. Kazak, and A. Ryzhevich, "A high-efficient method for generating radially and azimuthally polarized Bessel beams using biaxial crystals," Opt. Commun. **285**, 4807–4810 (2012).
128. J. Kalwe, M. Neugebauer, C. Ominde, G. Leuchs, G. Rurimo, and P. Banzer, "Exploiting cellophane birefringence to generate radially and azimuthally polarised vector beams," Eur. J. Phys. **36**, 025011 (2015).
129. R. A. Terborg, J. P. Torres, and V. Pruneri, "Technique for generating periodic structured light beams using birefringent elements," Opt. Express **26**, 28938–28947 (2018).
130. G. Piquero, L. Monroy, M. Santarsiero, M. Alonzo, and J. C. G. de Sande, "Synthesis of full Poincaré beams by means of uniaxial crystals," J. Opt. **20**, 065602 (2018).
131. J. C. G. de Sande, G. Piquero, M. Santarsiero, and F. Gori, "Partially coherent electromagnetic beams propagating through double-wedge depolarizers," J. Opt. **16**, 035708 (2014).
132. L. V. Alekseeva, I. V. Povkh, V. I. Stroganov, B. I. Kidyarov, and P. G. Pasko, "Four-ray splitting in optical crystals," J. Opt. Technol. **69**, 441 (2002).
133. V. Kuznetsov, D. Faleiev, E. Savin, and V. Lebedev, "Crystal-based device for combining light beams," Opt. Lett. **34**, 2856–2857 (2009).
134. C. Samlan and N. K. Viswanathan, "Generation of vector beams using a double-wedge depolarizer: non-quantum entanglement," Opt. Laser Eng. **82**, 135–140 (2016).